Jiafeng Xu
Centre for Research-based Innovation on Marine Operations (SFI MOVE), Department of Ocean Operations and Civil Engineering, Norwegian University of Science and Technology, NTNU, Aalesund NO-6009, Norway
e-mail: jiafeng.xu@ntnu.no

Zhengru Ren[1]
Centre for Research-based Innovation on Marine Operations (SFI MOVE), Centre for Autonomous Marine Operations and Systems (AMOS), Department of Marine Technology, Norwegian University of Science and Technology, NTNU, Trondheim NO-7491, Norway
e-mail: zhengru.ren@ntnu.no

Yue Li
Centre for Research-based Innovation on Marine Operations (SFI MOVE), Department of Ocean Operations and Civil Engineering, Norwegian University of Science and Technology, NTNU, Aalesund NO-6009, Norway
e-mail: yue.li@ntnu.no

Roger Skjetne
Centre for Research-based Innovation on Marine Operations (SFI MOVE), Centre for Autonomous Marine Operations and Systems (AMOS), Department of Marine Technology, Norwegian University of Science and Technology, NTNU, Trondheim NO-7491, Norway
e-mail: roger.skjetne@ntnu.no

Karl Henning Halse
Centre for Research-based Innovation on Marine Operations (SFI MOVE), Department of Ocean Operations and Civil Engineering, Norwegian University of Science and Technology, NTNU, Aalesund NO-6009, Norway
e-mail: karl.h.halse@ntnu.no

Dynamic Simulation and Control of an Active Roll Reduction System Using Free-Flooding Tanks With Vacuum Pumps

Ship roll motion is critical for offshore operations due to its lack of damping mechanism. This paper demonstrates a dynamic simulation scheme of an active roll reduction system using free-flooding tanks controlled by vacuum pumps. A tank is installed on each side of a catamaran. Both the tank hatches are opened to the sea and the air chambers of both tanks are connected by an air duct. Vacuum pumps and air valve stabilized the wave-induced roll motion by controlling the water levels in the tanks through a feedback controller. The catamaran is a dynamic model with single degree-of-freedom (DOF) in roll, and its hydrodynamic behavior is calculated using potential theory by SHIPX. The air chambers are modeled as isothermal processes of ideal gas. The behavior of the liquid flow in a tank is simulated by incompressible Reynolds-averaged Navier–Stokes solver with the volume of fluid model, then summarized as a response function for the vessel model. A simplified control plant model for the vacuum pumps is proposed where higher order behaviors are neglected and the external wave-induced load is unknown. A parameter-dependent observer and a backstepping controller are adopted to estimate the external load and to reduce the roll motion. The system stability is proved by Lyapunov's direct method. The performance of the entire system is evaluated in terms of roll reduction capability and power cost. The system is more suitable for roll reduction in low-speed or resting conditions. [DOI: 10.1115/1.4040235]

1 Introduction

Due to the lack of damping mechanism, ship roll motion is critical to various offshore operations, e.g., offshore wind turbine installation and subsea operations [1,2]. Excessive roll motion could cause both physiological and psychological issues such as acceleration-induced fatigue and cognitive impairment, as well as engineering issues such as structural failure and cargo damage. Passive roll reduction approaches such as bilge keel, fixed fins, free-surface tank, U-tank, and flopper stoppers have been proven their own strengths and weaknesses in numerous studies [3–5]. Active roll reduction systems such as active fins and pneumatic/hydraulic-pump-activated tanks are studied in Refs. [6] and [7]. This paper revisits the concept of free-flooding tanks with a pneumatic pump. The dynamic system is modeled with higher nonlinear characteristics and a feedback control law is adopted.

Frahm [8] first introduced the U-tank stabilization system as an improvement to the many disadvantages of free-surface tank. Based on Frahm's work, some modifications have removed the horizontal water channel on the bottom of the U-tank. As a result, the bottoms of the tanks are opened to the sea [7]. These so-called free-flooding tanks were retrofitted to six USN cruisers of *Pensacola* and *Northampton* classes during 1931–1932 and later in 1988

[1]Corresponding author.

Contributed by the Ocean, Offshore, and Arctic Engineering Division of ASME for publication in the JOURNAL OF OFFSHORE MECHANICS AND ARCTIC ENGINEERING. Manuscript received October 14, 2017; final manuscript received May 3, 2018; published online June 28, 2018. Assoc. Editor: Marcelo R. Martins.

Copyright © 2018 by ASME

Downloaded From: http://offshoremechanics.asmedigitalcollection.asme.org/ on 08/20/2018 Terms of Use: http://www.asme.org/about-asme/terms-of-use

to the aircraft carrier *USS Midway*. The air chamber on the top of each tank is connected by an air duct and controlled by a valve and an air pump. More recently, a Norwegian company *Marine Roll & Pitch Control* proposed a design where the air chambers of two tanks are isolated and controlled by individual pumps separately [9]. The design of free-flooding tanks is ideally suitable for multihulls, such as catamarans or trimarans, which have a longer leveling arm and subsequently less required volume for tanks. On the downside, the free-flooding tanks are susceptible to high cruising speed since the effective inlet flow is reduced due to pressure drop.

The target system in this paper is a free-flooding tank installed on each side of a catamaran. The tank hatches are opened downward into the sea. The air duct on the top of the chamber is connected to a vacuum pump. The pump is a part of a larger control system, which controls the air flow to both tanks. The inlet flow from one side is not necessarily equal to the outlet flow to the other side due to the requirement of the pressure levels in both tanks. The design is similar to the classical "N-tank" proposed by Bell and Walker [7]. Moaleji [10] modeled the system in a rather hydrostatic perspective and proposed an adaptive inverse controller. In this paper, more hydrodynamic features are added into the dynamic model and a more advanced nonlinear feedback controller is proposed.

2 Mathematical Modeling

2.1 Tanks. The tanks are simplified as two symmetric cuboids with a constant cross section profile and a hatch opening on the bottom of each tank; see Fig. 1. In the figure, N_{air} denotes the amount of air being transferred in/out of the tank, p_a is the atmospheric pressure, p'_a is the internal air pressure of the tank, A_{tank} is the cross section area of the tank, A_{hatch} refers to the opening area of the hatch, h_{hatch} denotes the water depth of the hatch, h_{water} is the water head height inside the tank from the hatch, V_{water} stands for the water volume inside the tank, y_{tank} is the lateral leveling arm of the tank measured from the middle line of the tank to the middle line plane of the catamaran, and p_{in} and p_{ext} are the pressure on the hatch interior and exterior, respectively. The hatch is considered to be a sharp-edged orifice. The flow rate across the hatch can be expressed as a basic turbulent flow model, i.e.,

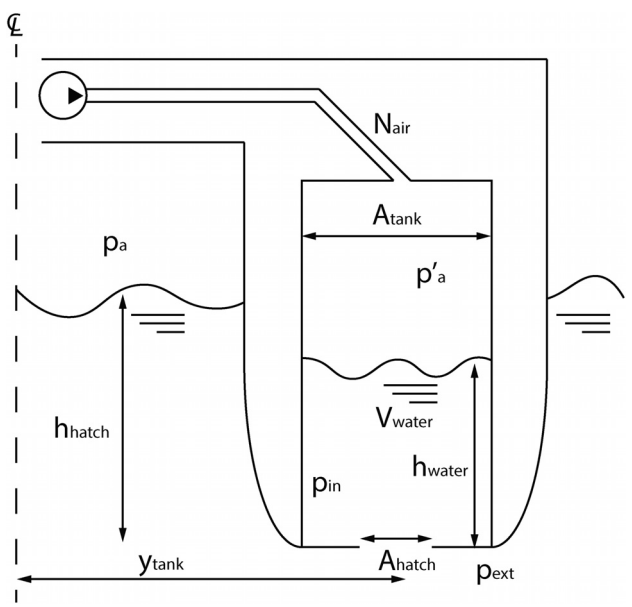

Fig. 1 Free-flooding tank of a catamaran

$$\dot{V}_{\text{water}} = \text{sgn}(\Delta p_{\text{hatch}}) C_d A_{\text{hatch}} \sqrt{\frac{2}{\rho}|\Delta p_{\text{hatch}}|} \tag{1}$$

where C_d is the discharge coefficient, ρ denotes water density, and $\Delta p_{\text{hatch}} = p_{\text{ext}} - p_{\text{in}}$ indicates the pressure difference between two sides of the hatch. The sign function $\text{sgn}(\cdot)$ is given by

$$\text{sgn}(a) = \begin{cases} 1 & \text{if } a > 0 \\ 0 & \text{if } a = 0 \\ -1 & \text{if } a < 0 \end{cases} \tag{2}$$

The external pressure p_{ext} is derived from Bernoulli's equation and consists of four components, i.e., the time-variant dynamic pressure of waves, hydrostatic pressure, pressure drop due to the hatch velocity, and atmospheric pressure

$$p_{\text{ext}} = \frac{\partial \Phi}{\partial t} + \rho g h_{\text{hatch}} + \frac{1}{2}\rho V_{\text{hatch}}^2 + p_a \tag{3}$$

where Φ is the fluid potential and V_{hatch} is the fluid velocity around the hatch exterior. In the world coordinate frame, V_{hatch} does not always equal to the hatch moving velocity, i.e., the movement of hatch in the water could cause an extra variation on the local fluid velocity and pressure field. According to Eq. (1), a downward movement during the inlet process could increase the external pressure due to the structure drag, which in turn increases the inlet flow; an upward movement during the outlet process creates a turbulence zone around the hatch exterior, decreases the external pressure, and increases the outlet flow, and vice versa. To sum up, the local fluid flow around the hatch is a complex fluid–structure interaction for which the combined effects of hatch movement and viscous structure drag cannot be easily quantified. Hence, the pressure variation term due to V_{hatch} is neglected in the absence of comprehensive in-loop computational fluid dynamics (CFD) simulations. The internal pressure p_{in} consists of two components, i.e., the internal hydrostatic pressure and compressed or expanded internal air pressure, that is

$$p_{in} = \rho(g - y_{\text{tank}}\ddot{\phi})h_{\text{water}} + p'_a \tag{4}$$

where Φ is the roll angle.

The internal hydrostatic pressure contains a variable acceleration term due to the weightlessness caused by the roll acceleration of the vessel. Hence, y_{tank} in Eq. (4) is used as lateral leveling arm of the tank. However, it causes the system state equation to be implicit. The internal air is assumed under the isothermal process of ideal gas. For a given initial pressure p_{init}, volume V_{init}, and the air transfer N_{air} in and out of the tank, the internal air pressure at any given moment is modeled as

$$p'_a = \left(\int_{t_0}^{t} \dot{N}_{\text{air}}\right) \Big/ (V_{\text{tank}} - V_{\text{water}}) \tag{5}$$

where V_{tank} denotes the total volume of the tank.

Typically, C_d is found around 0.6–1.0 for nozzles and orifices in a fluid system depending on the configuration and dimension. However, when the control system is activated, the fluid volume of both tanks oscillates around the equilibrium, as the flow across the hatch switches direction between inlet and outlet within a time frame similar to the wave periods, see Sec. 3. The waves in the North Sea are concentrated in a period range of 4–15 s, which is too short to be simplified as a time-invariant process without more detailed analysis. Additionally, the inlet flow is a process of filling up a closed empty space, while the outlet flow discharges the fluid into open environment. These two scenarios are not exactly opposite. Hence, necessary CFD calculations are carried out using STAR CCM+.

Downloaded From: http://offshoremechanics.asmedigitalcollection.asme.org/ on 08/20/2018 Terms of Use: http://www.asme.org/about-asme/terms-of-use

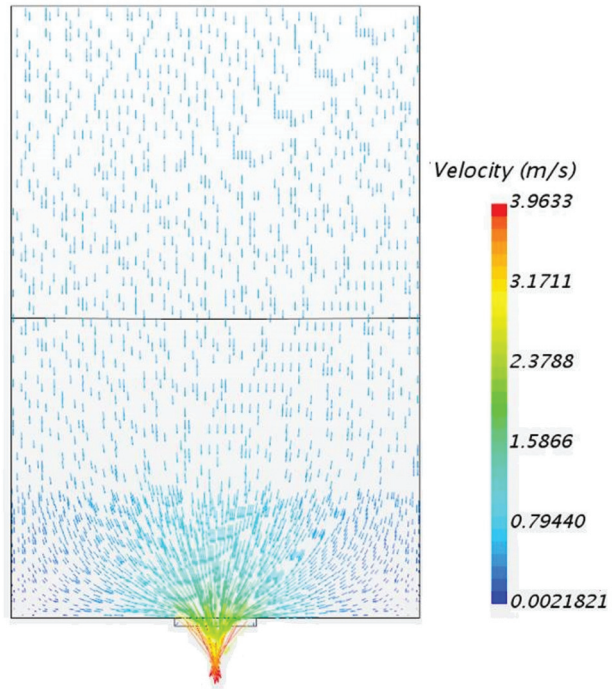

Fig. 2 Velocity field of the outlet flow, hatch area ratio 20%, and water head 0.9 m

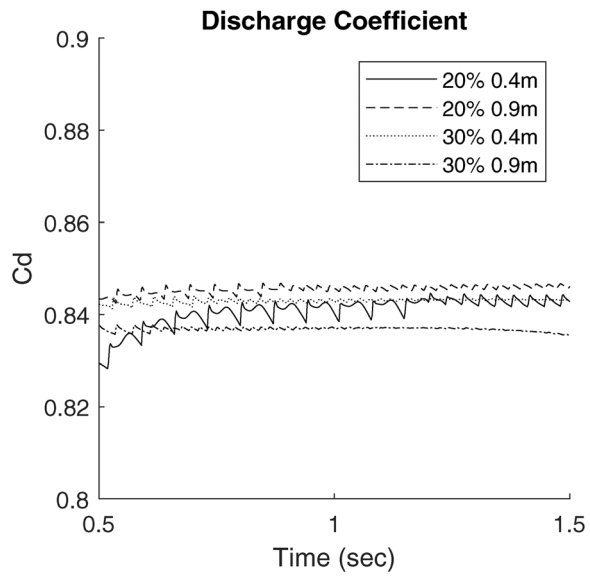

Fig. 3 Outlet discharge coefficients for different hatch areas and water heads

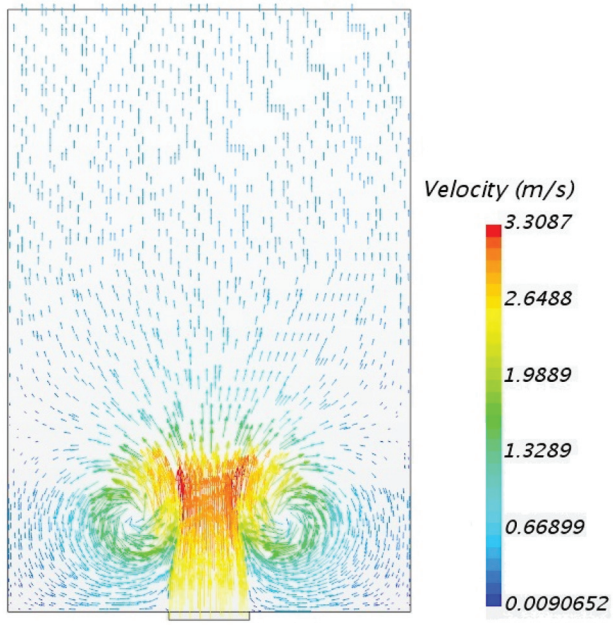

Fig. 4 Velocity field of inlet flow process, hatch area ratio 20%, and water head 0.9 m

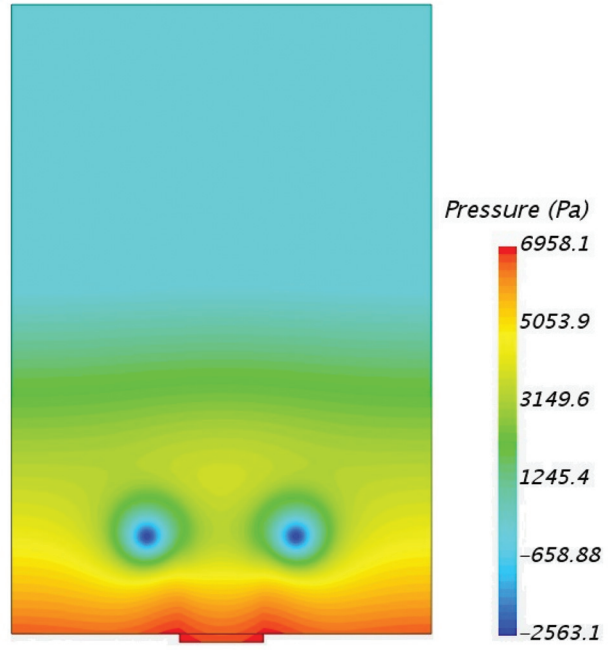

Fig. 5 Pressure of inlet flow process, hatch area ratio 20%, and water head 0.9 m

First, a CFD study is carried out in two-dimensional (2D) space and separated into two distinctive processes, i.e., inlet flow and outlet flow. The air inside a tank is treated as an ideal gas, and the water is incompressible with a constant external pressure. The multiphase flow is modeled using the volume fraction, and the turbulent flow is modeled by the standard K−ε model. For the outlet flow, Fig. 2 is an example of the velocity field with the hatch area ratio 20% and water head pressure difference 0.9 m, where no obvious vortex is detected. Figure 3 illustrates the outlet flow discharge coefficient $C_{d,}$ which holds almost a constant value around 0.84 for a variety of configurations.

In terms of the inlet flow, the internal pressure is calculated from the tank water head as in Eq. (4). Figures 4 and 5 present that two apparent vortices are detected in the vicinity of the hatch which creates extra low pressure areas. The three-dimensional (3D) CFD simulations are then conducted. A square hatch and a round hatch with the same characteristic length are studied, i.e., the edge of the square equals the diameter of the circle. The dimension of the cuboid tank is the same as that in the 2D study. Figure 6 shows the velocity distribution on the water surface during the inlet flow process. The comparison between round and square hatch, inlet and outlet, and 2D and 3D calculation is shown in Fig. 7. C_d fluctuates during the inlet due to the collapse and re-emergence of vortices, but 2D and 3D calculations on different

Downloaded From: http://offshoremechanics.asmedigitalcollection.asme.org/ on 08/20/2018 Terms of Use: http://www.asme.org/about-asme/terms-of-use

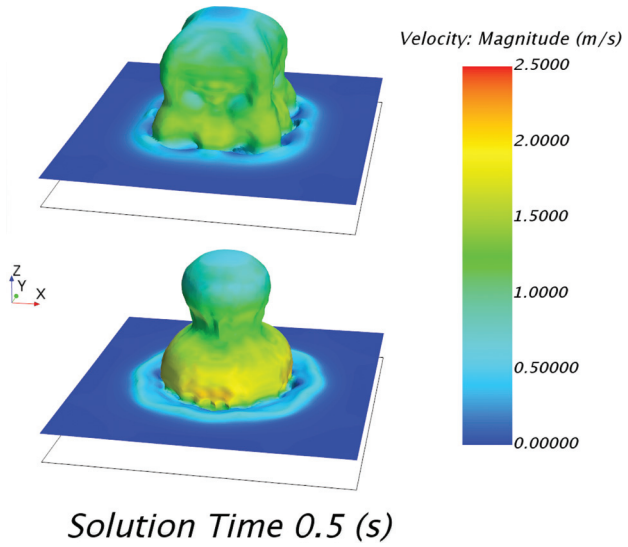

Fig. 6 Water surface under inlet flow process, hatch area ratio 20%, and water head 0.9 m

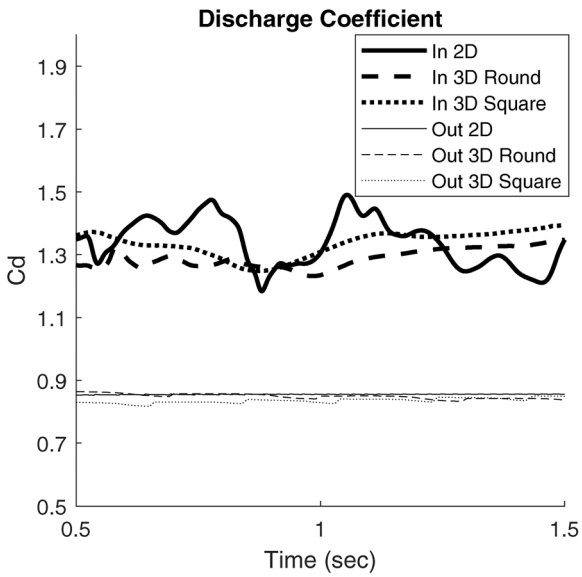

Fig. 7 Two-dimension and 3D discharge coefficients, hatch area ratio 20%, and water head ±0.9 m

hatch shapes show a consistent time average value of $C_d \approx 1.3$. In the outlet scenario, 3D calculation is consistent with the result from 2D calculation that $C_d \approx 0.84$.

In conclusion, CFD analysis reveals a time-variant C_d during a short-term inlet/outlet process. A disparity of C_d between the inlet and outlet flow processes is also noticed. Because the model is still under a strong linear approximation if Eq. (1) is used, C_d for inlet and outlet flows are assumed to be two distinctive time-invariant average values of the steady-states. The specific discharge coefficients for the inlet and outlet flow may still vary based on the shapes of the tanks and hulls, as well as other variables. The chosen $C_d \approx 1.3$ for inlet flow and $C_d \approx 0.84$ for outlet flow only serve as a reference for proof of concept in simulations. More accurate values must be retrieved on a case-by-case basis.

2.2 Pump. The vacuum pump is modeled as a linear system without time-delay effects and with a maximum power output. Since the pump does not always pump the air from the low pressure side to the high pressure side, a portion of the air transfers passively. The passive air transfer is controlled by a valve similar to Eq. (1) as

$$\dot{N}_{\text{passive}} = \text{sgn}(\Delta p_{\text{valve}}) C_d A_{\text{valve}} \sqrt{\frac{2}{\rho}|\Delta p_{\text{valve}}|} \tag{6}$$

where A_{valve} denotes the area of the valve, Δp_{valve} is the pressure difference between both sides of the valve, N_{passive} stands for the amount of air transferred passively due to Δp_{valve}, and the discharge coefficient C_d is approximated as 0.6 although more complex models exist [11]. The required extra air transfer is provided by the pump. The effective power required for the pump P_{pump} is calculated from the air transfer rate as

$$P_{\text{pump}} = (\dot{N}_{\text{air}} - \dot{N}_{\text{passive}}) \Delta p_{\text{valve}} / p'_a \tag{7}$$

2.3 Vessel. The target catamaran is simplified as a single degree-of-freedom (DOF) roll model. The governing equation is

$$(I + I_A(\infty) + \Delta I)\ddot{\phi}(t) + D(\infty)\dot{\phi}(t) + \int_0^t K(t-\tau)\dot{\phi}(t)d\tau + T\phi(t) = \tau_{\text{wave}}(t) + \tau_{\text{tank}}(t) \tag{8}$$

where I, $I_A(\infty)$, and ΔI are the moment of inertia, added moment of inertia, and varying moment of inertia due to the loss/gain of the water in the tanks, respectively, $D(\infty)$ refers to the linear damping coefficient, $K(t)$ is the fluid-memory effect [12], which is formulated by a state-space model [13], T indicates the linear restoring torque coefficient, and $\tau_{\text{wave}}(t)$ and $\tau_{\text{tank}}(t)$ are the torques exerted by the wave and the loss/gain of buoyancy from tanks on both sides. The internal fluid is considered to be bounded by the tank sides and moving with the catamaran. Hydrodynamics- related coefficients are generated in SHIPX vessel responses [14] using strip theory. The wave-induced moment is simulated with force response amplitude operator [13] and JONSWAP spectrum

$$\tau_{\text{wave}}(t) = \sum_i \bar{\tau}_i(\omega_i)\cos(\omega_i t + \varphi_i) \tag{9}$$

where $\bar{\tau}_i$, ω_i, and φ_i denote the response amplitude operator, wave frequency, and random phase of a specific wave component, respectively. The torque provided by the tanks τ_{tank} is given by

$$\tau_{\text{tank}} = \sum_{i=1,2} \rho g V_{\text{water},i} \left[\cos\phi y_{\text{tank},i} - \sin\phi\left(z_{hi} - \frac{V_{\text{water},i}}{A_{\text{hatch},i}}\right)\right] \tag{10}$$

where z_h is the height of the hatch.

3 Control Law

3.1 Problem Formulation. The control law is designed based on a simplified decoupled model where insignificant higher order behaviors are regarded as biases and noises [13,15]. The simplified model is summarized in the following equation, i.e.:

$$\dot{\phi} = p \tag{11a}$$

$$\dot{p} = \frac{1}{I_t}(-T\phi - Dp + \tau_{\text{tank}} + d) \tag{11b}$$

$$\dot{V}_{\text{water},1} = C_{v1}\text{sgn}(\Delta p_{h1})/\sqrt{|\Delta p_{h1}|} \tag{11c}$$

$$\dot{V}_{\text{water},2} = C_{v2}\text{sgn}(\Delta p_{h2})/\sqrt{|\Delta p_{h2}|} \tag{11d}$$

Downloaded From: http://offshoremechanics.asmedigitalcollection.asme.org/ on 08/20/2018 Terms of Use: http://www.asme.org/about-asme/terms-of-use

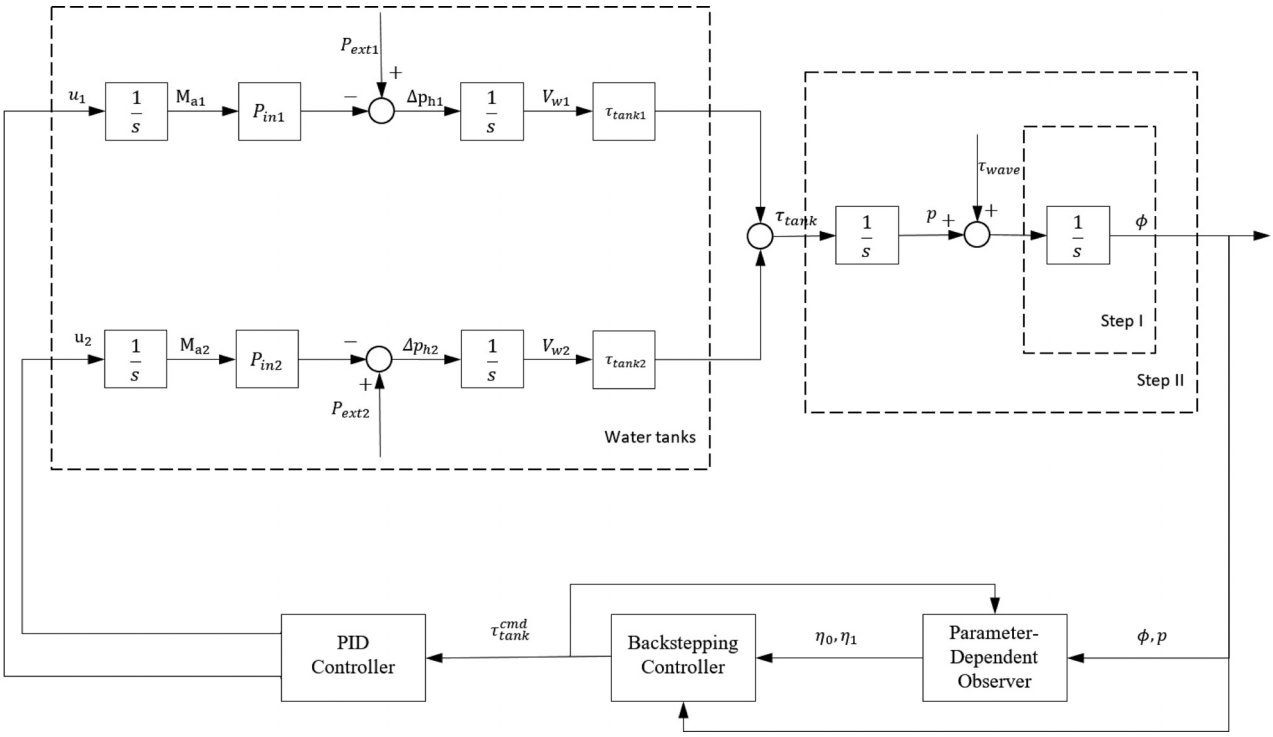

Fig. 8 Block diagram of the four-step backstepping controller

$$\dot{N}_{\text{air},1} = u_1 \tag{11e}$$

$$\dot{N}_{\text{air},2} = u_2 \tag{11f}$$

where the subscripts $i \in \{1, 2\}$ are the tank indices, $p = \dot{\phi}$ denotes the roll velocity, I_t stands for the total moment of inertia of the catamaran, $C_{vi} = C_{d,i}A_{\text{hatch},i}\sqrt{2/\rho}$ indicates the combined discharge coefficient, and u_i refers to the air transfer rate.

The slowly varying state d includes the wave-induced roll moment τ_{wave} and all sorts of biases, such as weightlessness effect in Eq. (4), fluid-memory effect, and moment of inertia variation of the tank in Eq. (8) [12,16].

The block diagram of the closed-loop system is presented in Fig. 8. The plant can be regarded as a cascade system. The control objective is to regulate the roll angle caused by the wave loads to zero by actively controlling the tanks, i.e., $\phi(t) \to 0$ as $t \to \infty$. The external disturbance d is important to the controller design because τ_{wave} is a main source of d. Because there is no existed wave-induced moment measurement for a vessel, it is difficult to cancel the term d during the control law design stage. Therefore, a parameter-dependent observer is applied to estimate the external disturbance d. Then the external disturbance, i.e., the wave-induced moment, is compensated in the backstepping process. A command signal is generated as the output of the backstepping control law. Then, a PID controller is used to track the command, i.e., $\tau_{\text{tank}}(u_1(t), u_2(t)) \to \tau_{\text{tank}}^{cmd}(t)$. The following assumptions are made:

(1) The volumes of the tanks are much smaller than the vessel. Therefore, we consider the total moment of inertia I_t is a constant with a rough initial estimate;
(2) An exosystem is assumed to be suitable to approximate the external disturbance and system uncertainty;
(3) The parameter-dependent observer does not monitor the frequency nor the amplitude of the wave. Hence, the system has tolerance to irregular waves.

LEMMA 1. *Consider the dynamic system* $\dot{\zeta} = G\zeta + bd$, *where* $\zeta \in \mathbb{R}^q$ *is the state, the pair (G, b) is controllable. Then, for any Hurwitz matrix* $G \in \mathbb{R}^{q\times q}$, *there exists a unique constant vector* $\psi \in \mathbb{R}$, *s.t., the disturbance d can be expressed in the form* $d = \psi^\top\zeta + \psi^\top\delta_d$, *and* $\dot{\delta}_d = G\delta_d$ *(see Ref. [17]).*

LEMMA 2. *(Rayleigh–Ritz theorem [18]). If the matrix* $A \in \mathbb{R}^{n\times n}$ *and vector* $x \in \mathbb{R}^n$ *are real, then*

$$\underline{\lambda}(A)\|x\|^2 \le z^\top Az \le \bar{\lambda}(A)\|x\|^2 \tag{12}$$

where $\underline{\lambda}(A)$ *and* $\bar{\lambda}(A)$ *are the smallest and largest eigenvalues of A.*

3.2 Parameter-Dependent Observer. Based on the famous internal model principle, reference signal or external disturbances can be asymptotically tracked if the external generator model is suitably reduplicated in the feedback path of the closed-loop control system [17]. The exosystem is given by

$$\dot{\chi} = \Gamma\chi \tag{13a}$$

$$d = l^\top\chi \tag{13b}$$

where $\chi \in \mathbb{R}^q$ is the state of the exosystem and $(\Gamma, l^\top)$ is assumed to be observable. Assume q is known, Γ and l are unknown, and χ and d are not measurable.

For the sake of simplification, a second-order exosystem is used in this paper to estimate the disturbance, i.e., $q = 2$. When d is not quite complex, second-order exosystem is the best choice because of its simplification. Higher-order exosystem is needed when $q = 2$ cannot estimate d well. The parameter-dependent observer is given by

$$d = \vartheta^\top\hat{\xi} + \psi^\top\delta \tag{14a}$$

where $\vartheta = [\psi^\top, \theta_1\psi^\top]^\top$ and $\xi = [(\eta_0 + v)^\top, \eta_1^\top]^\top$. The updating laws are given by

$$\dot{\eta}_0 = G\eta_0 + Gv(x) - bu \tag{14b}$$

$$\dot{\eta}_1 = G\eta_1 - \psi_1 \tag{14c}$$

Downloaded From: http://offshoremechanics.asmedigitalcollection.asme.org/ on 08/20/2018 Terms of Use: http://www.asme.org/about-asme/terms-of-use

where $b = [0, 1]^\top$ and $v(x) = [0, I_t p]^\top$. We refer the interested readers to Ref. [17] for detailed derivation.

3.3 Backstepping Control. Backstepping is a recursive control design for systems in strict feedback form Refs. [19] and [20]. The design process is illustrated as follows.

Define two new states

$$z_1 := \phi \tag{15}$$

$$z_2 := p - \alpha_1 \tag{16}$$

where α_1 is a vertical control.

The total control effort τ_{tank}^{cmd} is split into two parts

$$\tau_{\text{tank}}^{cmd} = u_y + u_d \tag{17}$$

where u_y responses to the path following, and u_d counteracts the disturbance d.

Step I. Select the control Lyapunov function as $V_1 = 1/2z_1^2$, and let

$$\alpha_1 = -c_1 z_1 \tag{18}$$

where c_1 is a positive gain constant. Substituting Eq. (11*a*) and Eq. (18) into V_1 yields

$$\dot{V}_1 = -c_1 z_1^2 + z_1 z_2 \tag{19}$$

Then, substituting Eqs. (16) and (18) into Eq. (11*a*), yields

$$\dot{z}_1 = -c_1 z_1 + z_2 \tag{20}$$

Step II. Substituting Eq. (11*b*) into the time derivative of Eq. (16) yields a new error state equation, which is given by

$$\dot{z}_2 = \frac{1}{I_t}\left(-T\phi - Dp + d + u_y + u_d\right) - \dot{\alpha}_1 \tag{21}$$

Construct a new control Lyapunov function

$$V_2 = V_1 + \frac{1}{2} z_2^2 \tag{22}$$

Differentiating Eq. (22) and substituting yield Eq. (21) yields

$$\dot{V}_2 = -c_1 z_1^2 + z_2\left[z_1 + \frac{1}{I_t}\left(-T\phi - Dp + d + u_y + u_d\right) - \dot{\alpha}_1\right] \tag{23}$$

Choose a virtual control as

$$u_y = T\phi + Dp + I_t(-z_1 + \dot{\alpha}_1 - c_2 z_2) \tag{24}$$

where c_2 is a positive gain constant. Substituting Eqs. (14*a*) and (24) into Eq. (21) yields

$$\dot{z}_2 = -z_1 - c_2 z_2 + \frac{1}{I_t}\left(\vartheta^\top \xi + \psi^\top \delta + u_d\right) \tag{25}$$

Then, u_d is designed as

$$u_d = -\hat{\vartheta}^\top \xi - \frac{z_2}{I_t} \tag{26}$$

where the hat operator $\hat{(\cdot)}$ denotes the estimated value. The adaptation law is chosen as

$$\dot{\hat{\vartheta}} = \frac{k_1}{I_t}\xi z_2 \tag{27}$$

where $k_1 > 0$ is the design parameter. Substituting Eq. (26) into Eq. (25) yields

$$\dot{z_2} = -z_1 - c_2 z_2 + \frac{1}{I_t}\left(\tilde{\vartheta}^\top \xi + \psi^\top \delta - \frac{z_2}{I_t}\right) \tag{28}$$

THEOREM 3. *Consider the closed-loop system consisting of the plant (11a) and (11b), uncertain exosystem (13), parameter-dependent observer (14), and adaptive regulator (24), (26), and (27) can stabilize the system, such that* $\phi \to 0$, *as* $t \to \infty$.

Proof. Define an error state, $\tilde{\vartheta} = \vartheta - \hat{\vartheta}$, where ϑ is assumed to be constant; therefore, $\dot{\tilde{\vartheta}} = -\dot{\hat{\vartheta}}$. Choose the Lyapunov function as

$$V = \frac{1}{2} z_1^2 + \frac{1}{2} z_2^2 + \frac{1}{2k_1}\tilde{\vartheta}^\top \tilde{\vartheta} + k_\delta \delta^\top P \delta \tag{29}$$

where $P = P^\top > 0$ satisfying $G^\top P + PG = -I$, and k_δ is larger than the maximum eigenvalue of the matrix $\psi\psi^\top$. Taking the time derivative of Eq. (29), using Lemma 1 and Lemma 2 leads to

$$\begin{aligned}
\dot{V} &= -c_1 z_1^2 - c_2 z_2^2 + \frac{z_2}{I_t}\tilde{\vartheta}\top\xi - \left(\frac{z_2}{I_t}\right)^2 + \frac{z_2}{I_t}\psi^\top\delta \\
&\quad - \frac{1}{k_1}\tilde{\vartheta}^\top\dot{\hat{\vartheta}} + k_\delta\delta^\top(G^\top P + PG)\delta \\
&= -c_1 z_1^2 - c_2 z_2^2 - \left(\frac{z_2}{I_t}\right)^2 + \frac{z_2}{I_t}\psi^\top\delta - k_\delta\delta^\top\delta \\
&\le -c_1 z_1^2 - c_2 z_2^2 - \left(\frac{z_2}{I_t}\right)^2 + \frac{z_2}{I_t}\psi^\top\delta - \left(\delta\psi^\top\right)^2 \\
&\le -c_1 z_1^2 - c_2 z_2^2 - \frac{3}{4}\left(\psi^\top\delta\right)^2 \le 0
\end{aligned}$$

when $\dot{V} = 0$, $z_1 = \dot{z}_1 = z_2 = \dot{z}_2 = \psi^\top\delta = 0$. From Eq. (28), $\tilde{\vartheta}$ has to be zero, if $\xi \neq 0$. From LaSalle-Yoshizawa theorem [19], every solution starting in $\{\Omega|\dot{V} = 0\}$ stays at the origin; therefore, $z_1 \to 0$, as $t \to \infty$. □

4 Numerical Case Study

To analyze the dynamic behavior of the entire system and the proposed control law, a numerical case study is set up in this section. The main system parameters are tabulated in Table 1. Instead of having a realistic parameter set, the parameters are chosen to serve a plausible starting point for the preliminary design. The system can provide its maximum counter torque when the tank on one side is completely emptied and the other one is full.

Table 1 System main parameters

Parameter	Value
Vessel length	100 m
Vessel breadth	42 m
Vessel depth	11 m
Vessel draft	9 m
Vessel mass	19345 ton
Vessel roll moment of inertia	3×10^9 kg/m^2
Wave height	2–5 m
Wave period	5–12 s
Tank length, width and height	(15–30)$\times$ 8 $\times$ 8 m
Tank torque arm	24 m
Hatch area	15 m^2
Valve area	1 m^2
Pump max. power	300 kW

Downloaded From: http://offshoremechanics.asmedigitalcollection.asme.org/ on 08/20/2018 Terms of Use: http://www.asme.org/about-asme/terms-of-use

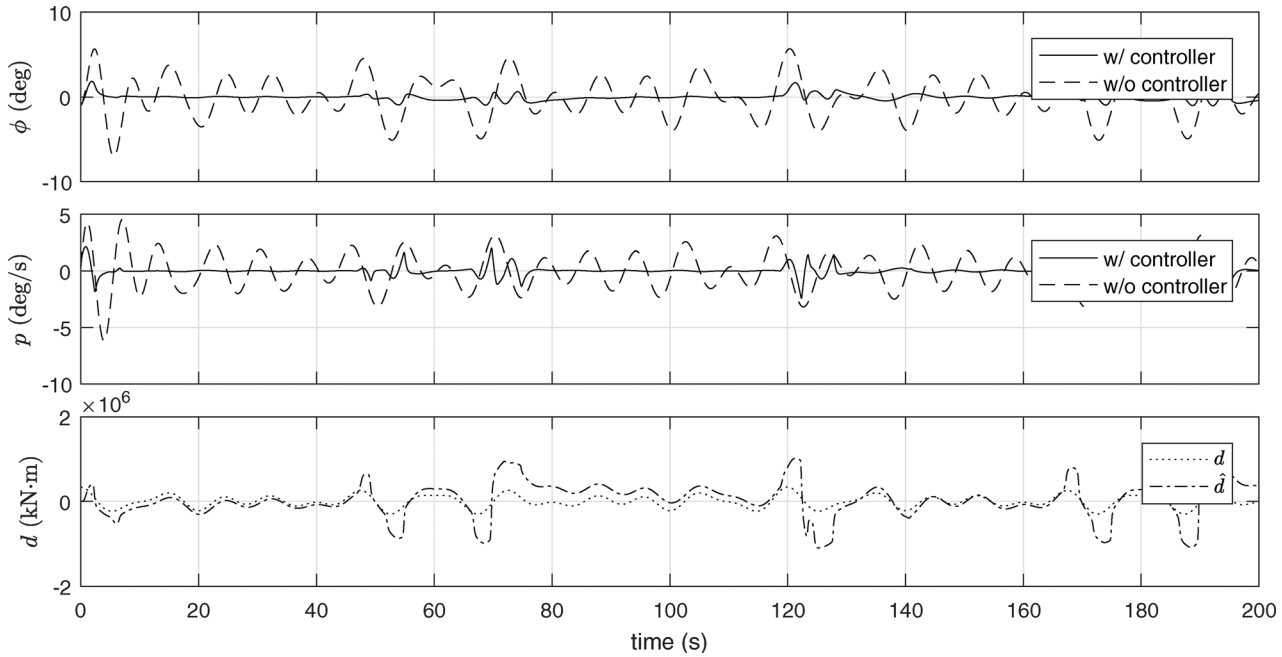

Fig. 9 Controller performance, ($H_s = 3.6$ m, $L_{\text{tank}} = 15$ m, and $T_p = 12$ s)

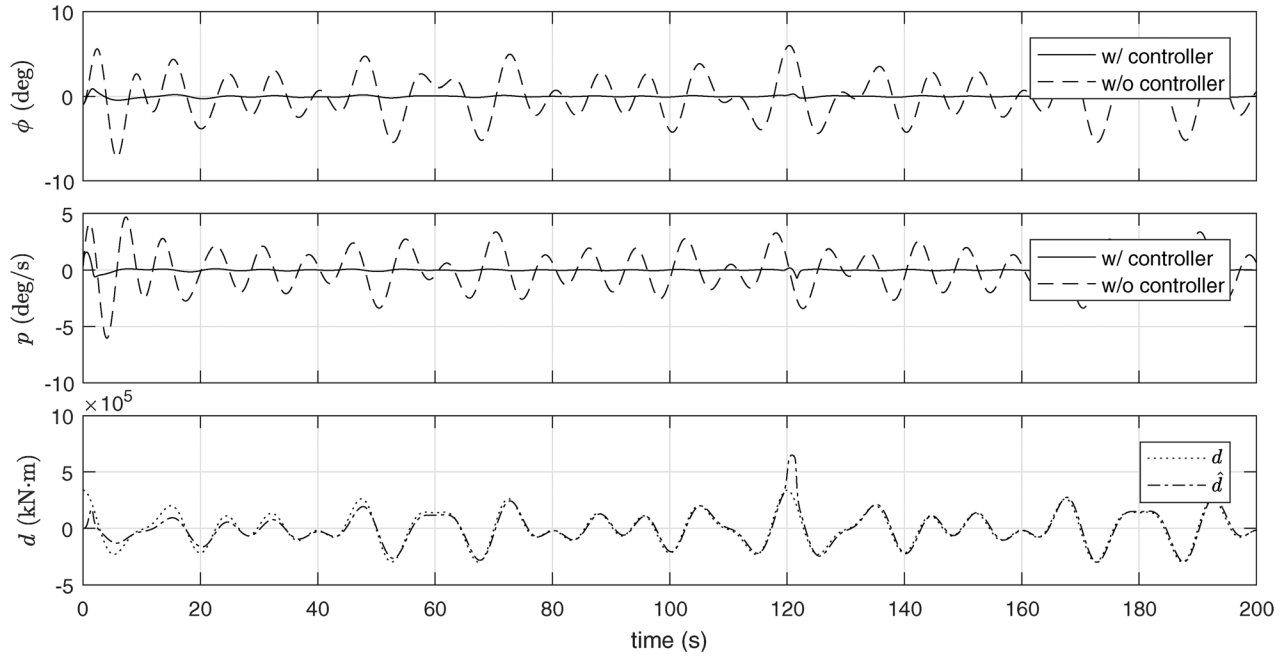

Fig. 10 Controller performance ($H_s = 3.6$ m, $L_{\text{tank}} = 20$ m, and $T_p = 12$ s)

4.1 Controller Performance. After a fine tuning process, Figs. 9–11 present the time domain simulation results in beam waves with different significant wave heights (H_s) and tank lengths (L_{tank}). The wave period (T_p) is 12 s. The first two subplots depict the vessel motion and velocity with and without the anti-roll controller. The third subplot shows the disturbance predicted by the observer comparing with the actual value. In order to generate the wave-induced torque τ_{wave} in the simulations, the corresponding JONSWAP spectral density is sampled at three frequencies. For a more realistic and detailed analysis of system performance under irregular sea state, a higher resolution wave spectrum shall be used.

With insufficient tank volume, the system cannot fully compensate the wave-induced vessel motion; see Fig. 9. The observer estimates the wave-induced disturbance quite well after the initialization period, but once the system capacity is overloaded, the observer needs time to reconverge. Figure 10 illustrates an improved performance after the tank length is increased from 15 m to 20 m. The controller largely reduces the amplitude of the roll motion. During the simulations, the influence of the changing

Downloaded From: http://offshoremechanics.asmedigitalcollection.asme.org/ on 08/20/2018 Terms of Use: http://www.asme.org/about-asme/terms-of-use

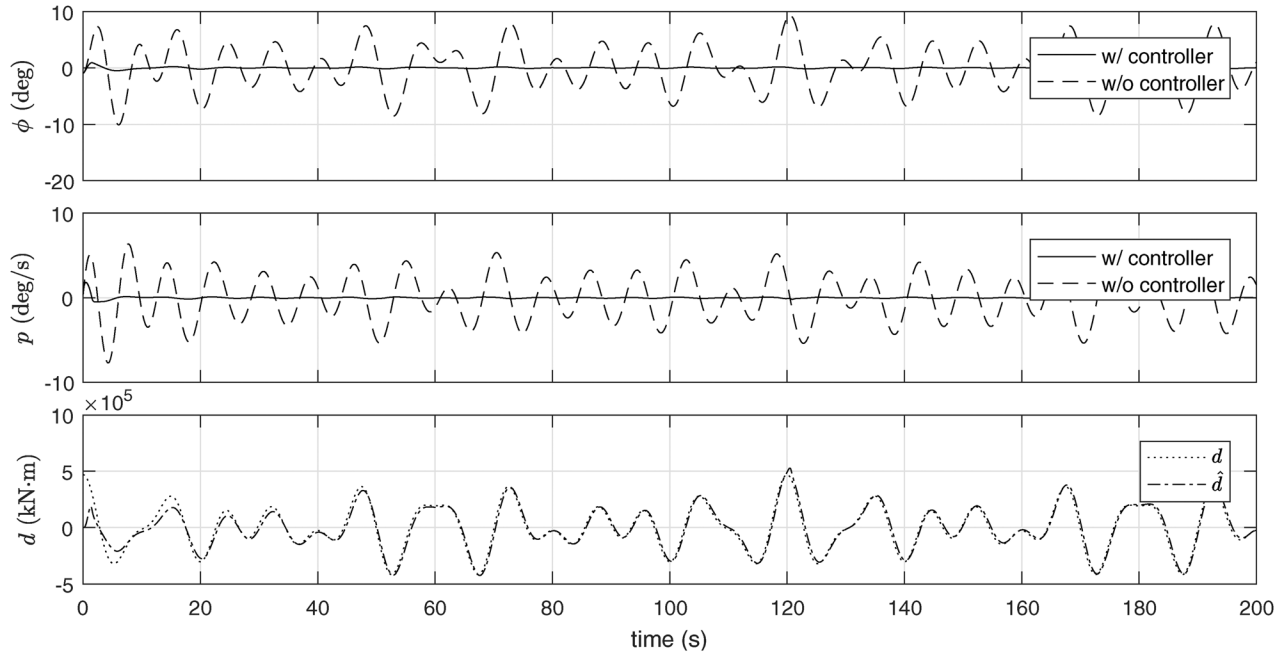

Fig. 11 Controller performance ($H_s = 5$ m, $L_{tank} = 30$ m, and $T_p = 12$ s)

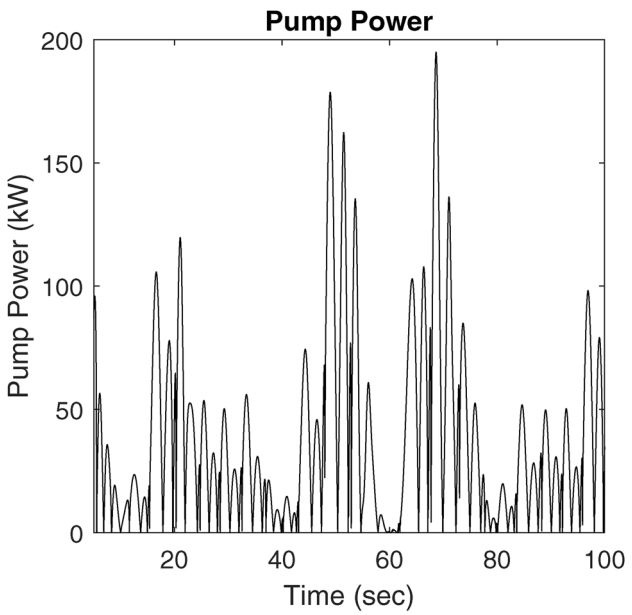

Fig. 12 Pump power output ($H_s = 5$ m, $L_{tank} = 30$ m, and $T_p = 12$ s)

moment of inertia caused by the tanks is not remarkable. Figure 11 presents the performance in a severe wave condition, an even larger tank is still theoretically possible. However, an over-sized anti-roll tank will surely cause other design problems. Note that the roll reduction is not perfect. Increasing the control gains in the backstepping and PID controllers are helpful to make the control more responsive. On the other hand, the control gains are directly determined by the control cost and physical capability of the actuators.

4.2 Pump Capacity. Figure 12 shows the pump power output fluctuation while the catamaran is under control. Such fast, responsive, and large pump capacity can be composed by several smaller pumps for both control redundancy and design flexibility, such as Panther WA 3032-3300D series, WT 0100-0730 series, and Samos SB 0050-1400 series from *Busch Vacuum Pumps and Systems*. Figure 13 shows the results of the vessel roll response in frequency domain under different pump capacities. The 100% line is actually conducted with unlimited pump power. The target catamaran has a very low natural period of roll due to its large breadth. Even with unlimited power, the system cannot fully compensate the wave induced roll motion. Also, the smaller the wave period is, the higher the energy it carries, and less action time is available for the system. As the wave period increases, the effect of the proposed anti-roll system improves, resulting in a greater amplitude reduction from uncontrolled motion.

There are many other parameters that significantly influence the simulation results and system efficiency. If the hatch area is too small, greater pressure difference around the hatch is required to achieve the desired water flow, which can only be achieved by having a more powerful pump to create greater air pressure change in a certain time period. If the hatch is too large, the passive movement of tank waters may be out of phase with the vessel motion, despite the increasing structural vulnerability. However, this causes a decreased capability of passive control and increased the demand for active pump power.

The same principle applies to the design of air duct and valve. The diameter of the duct and dimension of the valve need to be carefully designed to maximize the passive capability of the system. For severe sea state, bigger tanks are necessary to provide enough maximum counter torque. Larger lever arms provide greater torque without occupying extra space onboard. The catamaran is designed for offshore wind turbine installations, motivating the greater breadth and low speed. The studied system is suitable for similar working conditions such as offshore heavy lifting and anchor handling. In special cases, the existing ballast water tanks can be modified into the proposed *N*-tank without significant structural modification.

5 Conclusions

This paper demonstrates a dynamic simulation scheme of an active roll reduction system using free-flooding tanks controlled

Downloaded From: http://offshoremechanics.asmedigitalcollection.asme.org/ on 08/20/2018 Terms of Use: http://www.asme.org/about-asme/terms-of-use

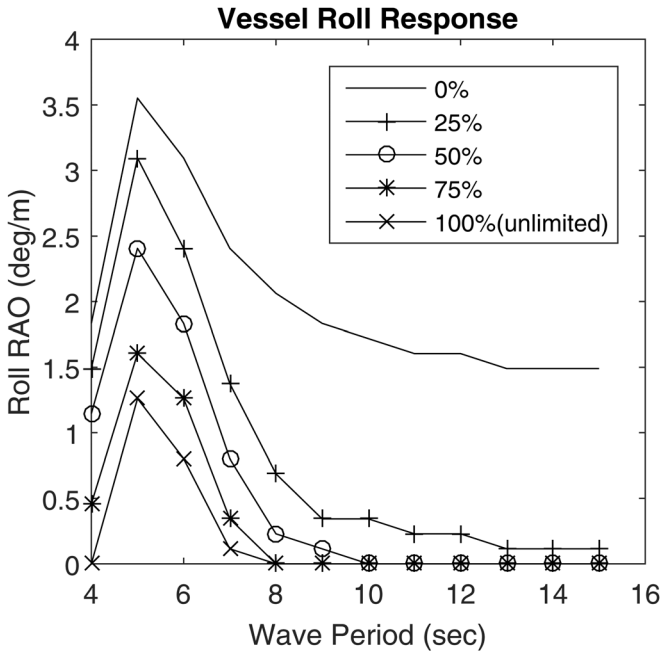

Fig. 13 Vessel roll response ($H_s = 5$ m, $L_{tank} = 30$ m, and $T_p = 12$ s)

by vacuum pumps, with a parameter-dependent observer and a backstepping controller. Free-flooding tanks at both sides of the catamaran are open to the sea without air duct in between. Vacuum pumps with active stabilization controller provide optimal filling in these tanks based on input from the ship movement. The ship is simulated as a dynamic model with a single degree-of-freedom in roll. A control design model is derived for the vacuum pumps. The stability is proved by Lyapunov's direct method and LaSalle-Yoshizawa theorem. For vessels which operate mostly at low speed and a relatively calm sea state, the proposed roll reduction system provides great performance with minor cost. Future application areas of proposed motion control system can be offshore installation vessels and floating wind turbines integrated with the dynamic positioning system [21–23]. Bigger tank is required for severe sea state. More detailed study about the design will be carried out with relevant companies.

Acknowledgment

This research is supported by Marine Roll & Pitch Control AS. Similar designs from this company have been employed on multiple vessels.

Funding Data

- Norges forskningsråd Research Council of Norway (RCN) Project No. 237929: CRI MOVE and RCN Project No. 223254: CoE NTNU AMOS.

References

[1] Ren, Z., Jiang, Z., Skjetne, R., and Gao, Z., 2018, "An Active Tugger Line Force Control Method for Single Blade Installations," Wind Energy. (under review).
[2] Veritas, D. N., 2011, "Modelling and Analysis of Marine Operations," Det Norske Veritas, Oslo, Norway, Report No. DNV-RP-H103.
[3] Moaleji, R., and Greig, A. R., 2005, "On the Development of Ship Anti-Roll Tanks," Ocean Eng., **34**(1), pp. 103–121.
[4] Marzouk, O. A., and Nayfeh, A. H., 2009, "Control of Ship Roll Using Passive and Active Anti-Roll Tanks," Ocean Eng., **36**(9–10), pp. 661–671.
[5] Jiang, Z., Acero, W. G., Gao, Z., and Li, L., 2017, "A Numerical Study on a Flopper Stopper for Leg Positioning of a Jack-Up Barge," ASME Paper No. OMAE2017-62034.
[6] Vasta, J., Gidding, A., Taplin, A., and Stilwell, J., 1961, "Roll Stabilization by means of Passive Tanks," Trans. Soc. Nav. Archit. Mar. Eng., **69**, p. 411.
[7] Bell, J., and Walker, P., 1966, "Activated and Passive Controlled Fluid Tank System for Ship Stabilization," Trans. Soc. Nav. Archit. Mar. Eng., **74**, p. 150.
[8] Frahm, H., 1911, "Results of Trails of the Anti-Rolling Tanks at Sea," Trans. Inst. Nav. Archit., **23**(1), pp. 571–597.
[9] Halse, K. H., Asoy, V., and Sporsheim, O., 2012, "An Active Roll Reduction System Using Free Flooding Tanks Controlled by Vacuum Pumps," World Maritime Technology Conference, Saint-Petersburg, Russia, May 29–June 1.
[10] Moaleji, R., 2006, "Adaptive Control for Ship Roll Stabilization Using Anti-Roll Tanks," Ph.D. thesis, University College London, London.
[11] ASME, 2001, *Measurement of Fluid Flow Using Small Bore Precision Orifice Meters*, American Society of Mechanical Engineers, New York.
[12] Cummins, W., 1962, "The Impulse Response Function and Ship Motions," Skispsteknish Forskningsinstitutt, Washington, DC, Report No. 1661.
[13] Fossen, T. I., 2011, *Handbook of Marine Craft Hydrodynamics and Motion Control*, Wiley, Trondheim, Norway.
[14] Fathi, D., and Hoff, J. R., 2004, *ShipX Vessel Responses (VERES) Theory Manual*, MARINTEK A/S, Norway.
[15] Perez, T., and Blanke, M., 2010, "Ship Roll Motion Control," Eighth IFAC Conference on Control Applications in Marine Systems, Rostock, Germany, Sept. 15–17.
[16] Bergdahl, L., 2009, "Wave-Induced Loads and Ship Motions," Chalmers University of Technology, Göteborg, Sweden, Technical Report No. 2009:1.
[17] Nikiforov, V. O., 1998, "Adaptive Non-Linear Tracking With Complete Compensation of Unknown Disturbances," Eur. J. Control, **4**(2), pp. 132–139.
[18] French, M., Szepesvári, C., and Rogers, E., 2003, *Performance of Nonlinear Approximate Adaptive Controllers*, Wiley, Hoboken, NJ.
[19] Khalil, H. K., 1996, *Nonlinear Systems*, Vol. 3, Prentice Hall, Upper Saddle River, NJ.
[20] Skjetne, R., and Fossen, T. I., 2004, "On Integral Control in Backstepping: Analysis of Different Techniques," American Control Conference (ACC), Boston, MA, June 30–July 2, pp. 1899–1904.
[21] Jiang, Z., Ren, Zhengru, G. Z., Sandvik, P. C., Halse, K. H., and Skjetne, R., 2018, "Mating Control of a Wind Turbine Tower-Nacelle-Rotor Assembly for a Catamaran Installation Vessel," The 28th International Ocean and Polar Engineering Conference, Hokkaido, Japan, June 10–15.
[22] Jiang, Z., Moan, T., and Gao, Z., 2015, "A Comparative Study of Shutdown Procedures on the Dynamic Responses of Wind Turbines," ASME J. Offshore Mech. Arct. Eng., **137**(1), p. 011904.
[23] Ren, Z., Skjetne, R., and Hassani, V., 2015, "Supervisory Control of Line Breakage for Thruster-Assisted Position Mooring System," IFAC-PapersOnLine, **48**(16), pp. 235–240.

Downloaded From: http://offshoremechanics.asmedigitalcollection.asme.org/ on 08/20/2018 Terms of Use: http://www.asme.org/about-asme/terms-of-use